Supporting Information for Methane Adsorption and Self-Diffusion in Shale Kerogen and Slit Nanopores by Molecular Simulations

Stéphane Tesson[†,‡] and Abbas Firoozabadi[*,†]

†*Reservoir Engineering Research Institute, 595 Lytton Avenue, Suite B., Palo Alto, CA 94301, USA*

‡*Department of Chemical and Environmental Engineering, University of California Riverside, Riverside, CA 92521, USA*

E-mail: abbas.firoozabadi@yale.edu

Phone: +1 (650) 326-9172

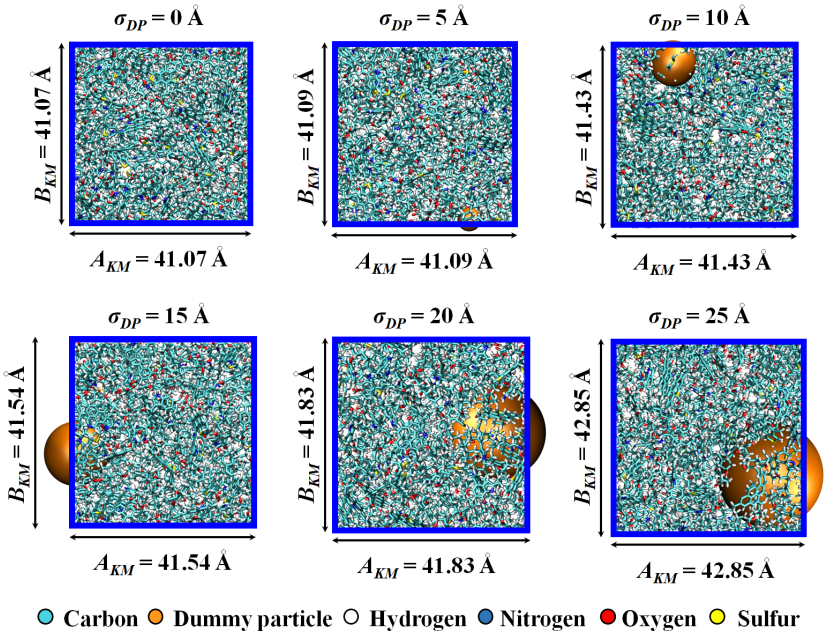

Figure S1: Final configurations from the molecular dynamics relaxation of kerogen matrices with dummy particle of size 0, 5, 10, 15, 20 and 25 Å at $T = 300$ K and $P = 1$ atm.

Table S1: Composition and structural parameters of the type II-A kerogen macromolecule adapted from Ungerer *et al.*[1]

Composition & structural properties	Experimental	Model
H/C	1.17	1.17
O/C	0.097	0.095
N/C	0.029	0.024
S/C	0.014	0.012
% of aromatic carbon from X-ray photoelectron spectroscopy	40	71
Average number of C atoms per aromatic cluster	12	11.4
Fraction of aromatic carbons with attachments (sp^3 C, N, S, O)	0.43	0.46
Protonated aromatic carbons (per 100 C)	13	14
Number of O in C-O per 100 C	5.0	5.2
Number of O in carboxylic groups (-COOH) per 100 C	1.3	1.6
Number of O in carboxylic groups (>C=O) per 100 C	3.4	2.8
Pyrrolic (mol % of N)	52	66
Pyridinic (mol % of N)	27	17
Quaternary (mol % of N)	18	17
Amino (mol % of N)	4	0
Aromatic S (% of organic S)	46	67
Aliphatic S (sulfides and thiols) (% of organic S)	54	33

Table S2: Pressure effect on kerogen matrix characteristics. The nitrogen probe particle is used to estimate the porosity and the accessible surface area at $T = 300$ K.

Dummy particle diameter [Å]	Pressure [atm]	Lattice parameters [Å]	Density [g.cm^{-3}]	Porosity [%]	Accessible surface area [m^2.g^{-1}]	Largest pore radius [Å]
5	1	41.09 ± 0.05	1.12 ± 0.01	0.13 ± 0.02	38 ± 5	3.29 ± 0.03
	50	41.08 ± 0.05	1.12 ± 0.01	0.10 ± 0.02	33 ± 4	3.34 ± 0.03
	100	41.03 ± 0.05	1.12 ± 0.01	0.12 ± 0.02	36 ± 5	3.36 ± 0.03
	150	41.00 ± 0.05	1.12 ± 0.01	0.11 ± 0.02	33 ± 5	3.39 ± 0.03
10	1	41.43 ± 0.05	1.09 ± 0.01	0.66 ± 0.13	91 ± 6	4.55 ± 0.05
	50	41.43 ± 0.07	1.09 ± 0.01	0.59 ± 0.11	85 ± 6	4.55 ± 0.05
	100	41.40 ± 0.05	1.09 ± 0.01	0.61 ± 0.07	91 ± 6	4.51 ± 0.05
	150	41.40 ± 0.05	1.09 ± 0.01	0.61 ± 0.07	85 ± 6	4.53 ± 0.04
15	1	41.54 ± 0.06	1.08 ± 0.01	1.19 ± 0.07	105 ± 6	6.06 ± 0.06
	50	41.49 ± 0.05	1.09 ± 0.01	1.18 ± 0.08	99 ± 6	6.09 ± 0.06
	100	41.45 ± 0.05	1.09 ± 0.01	1.17 ± 0.08	98 ± 5	6.06 ± 0.06
	150	41.44 ± 0.05	1.09 ± 0.01	1.18 ± 0.08	100 ± 6	6.05 ± 0.06
20	1	41.83 ± 0.06	1.06 ± 0.01	2.39 ± 0.09	174 ± 8	7.24 ± 0.07
	50	41.80 ± 0.06	1.06 ± 0.01	2.36 ± 0.07	174 ± 7	7.24 ± 0.07
	100	41.82 ± 0.05	1.06 ± 0.01	2.37 ± 0.09	168 ± 8	7.22 ± 0.07
	150	41.72 ± 0.06	1.07 ± 0.01	2.36 ± 0.09	165 ± 8	7.18 ± 0.07
25	1	42.85 ± 0.07	0.99 ± 0.01	4.1 ± 0.2	341 ± 13	7.96 ± 0.08
	50	42.82 ± 0.06	0.99 ± 0.01	3.8 ± 0.02	332 ± 12	7.99 ± 0.08
	100	42.78 ± 0.05	0.99 ± 0.01	4.0 ± 0.02	329 ± 13	7.96 ± 0.08
	150	42.79 ± 0.06	0.99 ± 0.01	3.9 ± 0.02	329 ± 13	7.96 ± 0.08

Table S3: Structure characterization. Porosity and accessible surface area are calculated from nitrogen probe particles at $T = 300$ K and $P = 1$ atm.

Dummy particle diameter [Å]	Lattice parameters [Å]	Density [g.cm^{-3}]	Porosity [%]	Nitrogen accessible surface area [m^2.g^{-1}]	Largest pore radius [Å]
0	41.07 ± 0.04	1.12 ± 0.01	0.02 ± 0.01	13 ± 3	2.69 ± 0.01
5	41.09 ± 0.05	1.12 ± 0.04	0.13 ± 0.02	39 ± 5	3.29 ± 0.01
10	41.43 ± 0.05	1.09 ± 0.04	0.66 ± 0.06	92 ± 6	4.55 ± 0.01
15	41.54 ± 0.05	1.08 ± 0.04	1.19 ± 0.07	105 ± 6	6.06 ± 0.01
20	41.83 ± 0.06	1.06 ± 0.04	2.39 ± 0.09	174 ± 6	7.24 ± 0.01
25	42.85 ± 0.07	0.99 ± 0.04	4.1 ± 0.2	341 ± 13	7.96 ± 0.01

The excess adsorption is not a monotonically increasing function of pressure. First, the excess adsorption increases. Then, it reachs a maximum, and finally decreases. The excess adsorption in Figure S4 is calculated by

$$n^{Exc} = n^{Ads} - V_{Acc} \times \rho_{Bulk}, \tag{1}$$

where n^{Exc} is the excess adsorption, V_{Acc} is the accessible volume by the adsorbate, and ρ_{Bulk} is the adsorbate bulk density[2] at a specific temperature and pressure.

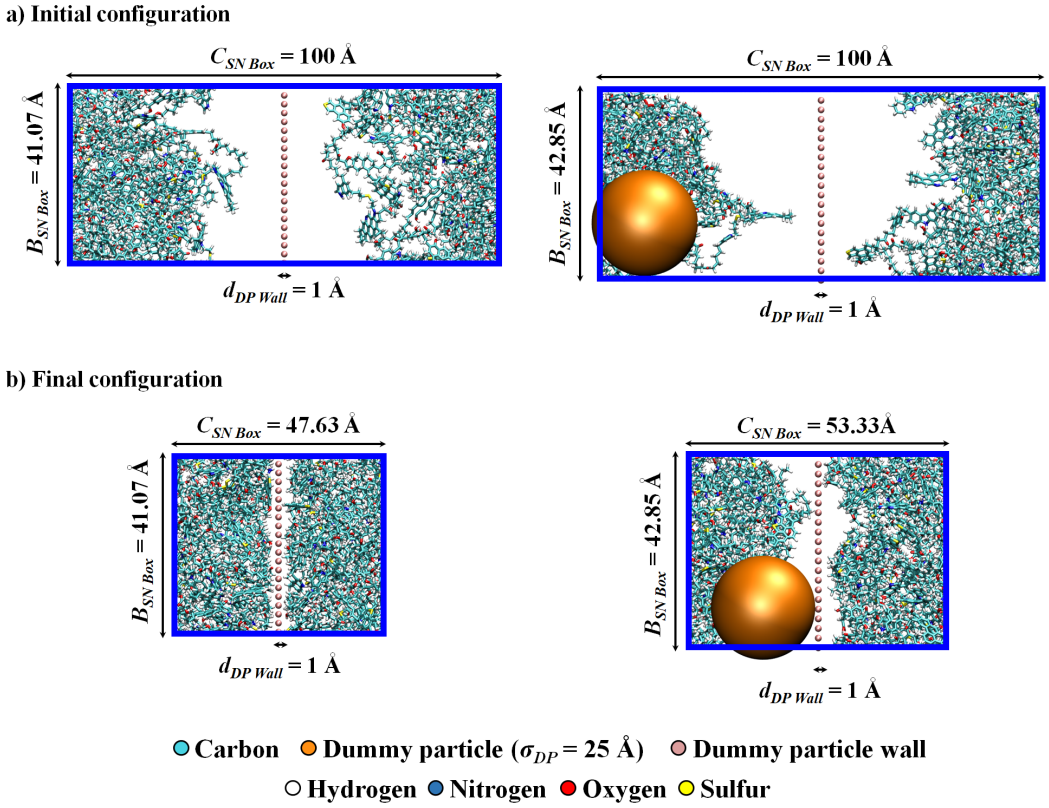

Figure S2: Configurations from molecular dynamics relaxation of systems with the dummy particle wall: a) initial configuration, and b) final configuration at $T = 300$ K and $P = 1$ atm.

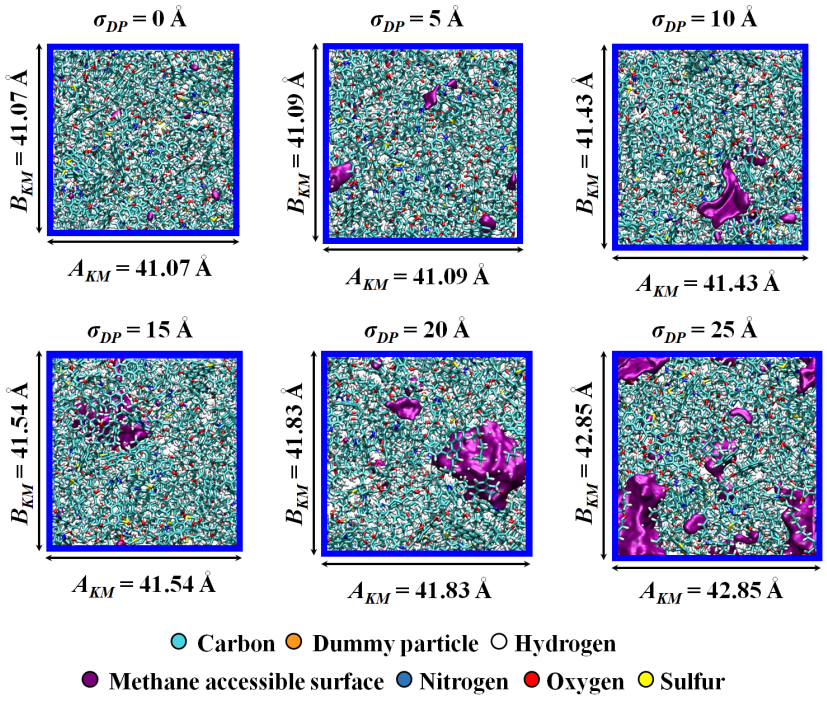

Figure S3: Methane accessible surfaces (in purple) of kerogen matrices at $T = 300$ K and $P = 1$ atm.

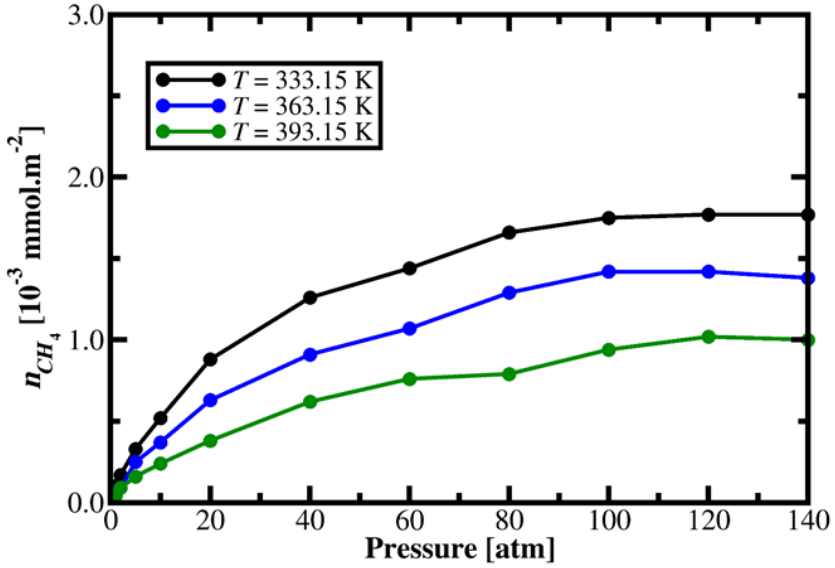

Figure S4: Methane excess adsorption in rigid kerogen matrix at different temperatures.

The absolute adsorption is fitted to the Langmuir model,

$$n^{Ads} = n^{Ads}_{max} \times \left(\frac{A_1 \times P}{1 + A_1 \times P} \right), \tag{2}$$

where n^{Ads} is the absolute adsorption, n^{Ads}_{max} is the Langmuir Maximum Adsorption (LMA), A_1 is the Langmuir constant and, P is the pressure.

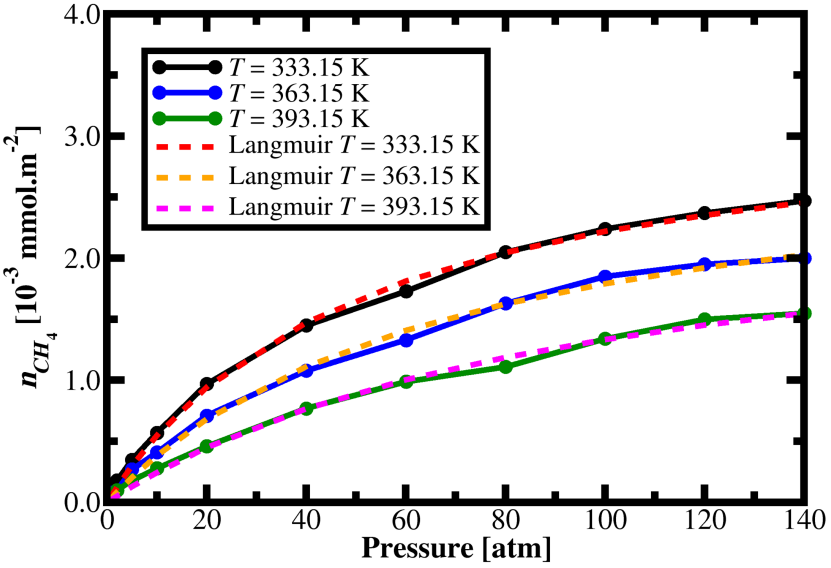

Figure S5: Methane absolute adsorption described by the Langmuir model at different temperatures.

The methane absolute adsorptions follow the Langmuir type I isotherm. The Langmuir maximum adsorption (n^{Ads}_{max}) is, repectively, equal to 3.3514×10^{-3}, 3.0212×10^{-3} and 2.6179×10^{-3} mmol.m^{-2}, and the Langmuir constant (A_1) is, repectively, equal to 0.0196, 0.0146 and 0.0103 atm^{-1}, at T = 333.15, 363.15 and 393.15 K. The Langmuir maximum adsorption and the Langmuir constant decrease with increasing temperature. Experimental[3–5] and computational[6–8] studies on shales, kerogens and coals show the same trend as the Langmuir model.

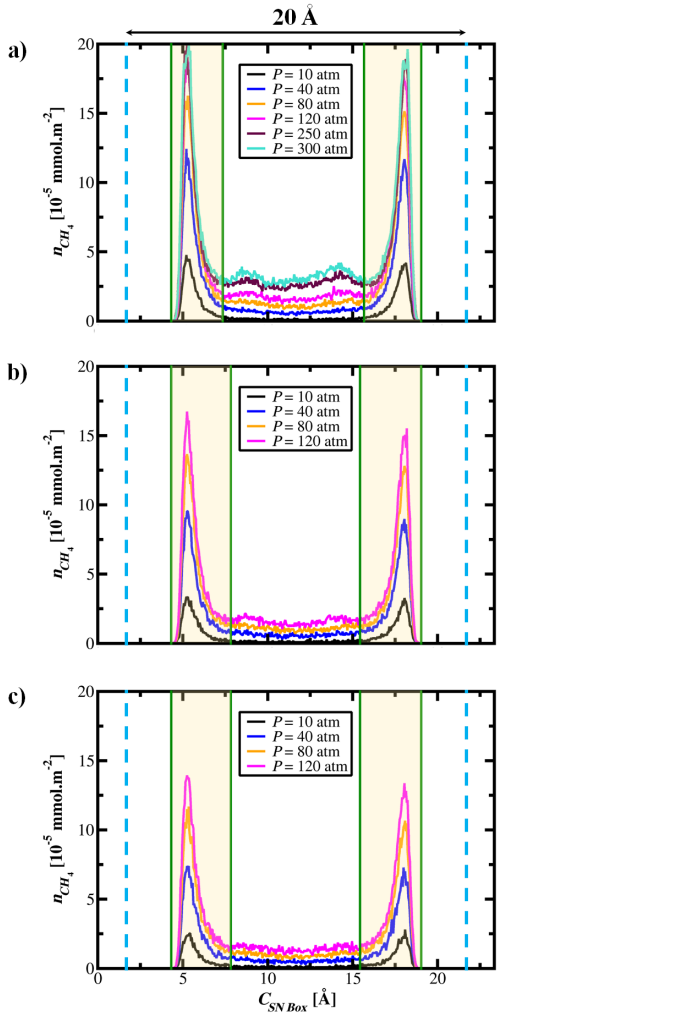

Figure S6: Density profiles of methane in the smooth slit nanopore at various pressures. a) $T = 333.15$ K, b) $T = 363.15$ K, and c) $T = 393.15$ K.

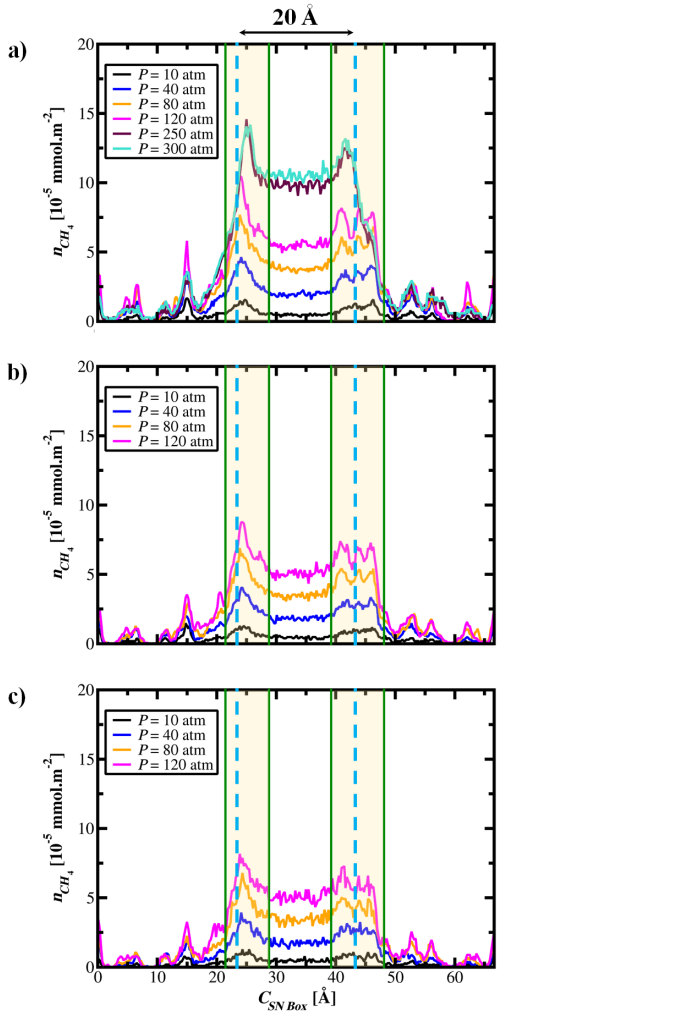

Figure S7: Density profiles of methane in the moderately rough rigid slit nanopore at various pressures. a) $T = 333.15$ K, b) $T = 363.15$ K, and c) $T = 393.15$ K.

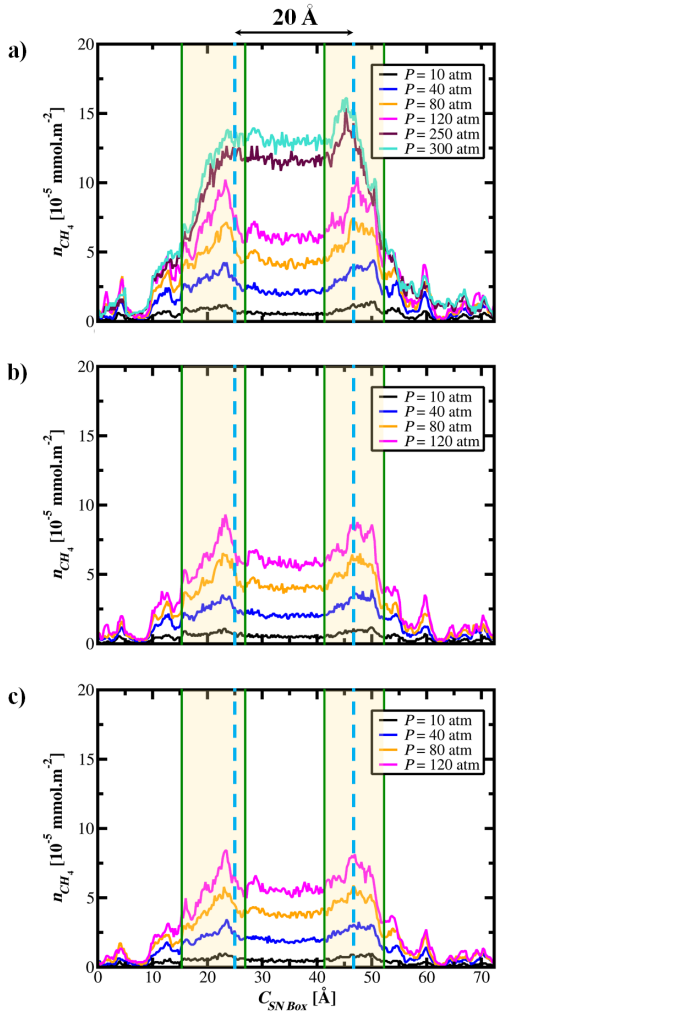

Figure S8: Density profiles of methane in the rough rigid slit nanopore at various pressures. a) $T = 333.15$ K, b) $T = 363.15$ K, and c) $T = 393.15$ K.

The absolute adsorption normalized by the accessible volume in the adsorption layer are plotted in Figures S9a, S9b, and S9c. The accessible volume in the adsorption layer for the rigid smooth slit nanopore, the moderately rough rigid slit nanopore, and rough rigid slit nanopore is, respectively, 11349.5 Å^3, 15756.6 Å^3, and 18101.7 Å^3. Figure S9 show that the surface chemistry may play an important role in the methane adsorption. Figure S9 also show that the surface roughness may affect the methane adsorption at high pressure.

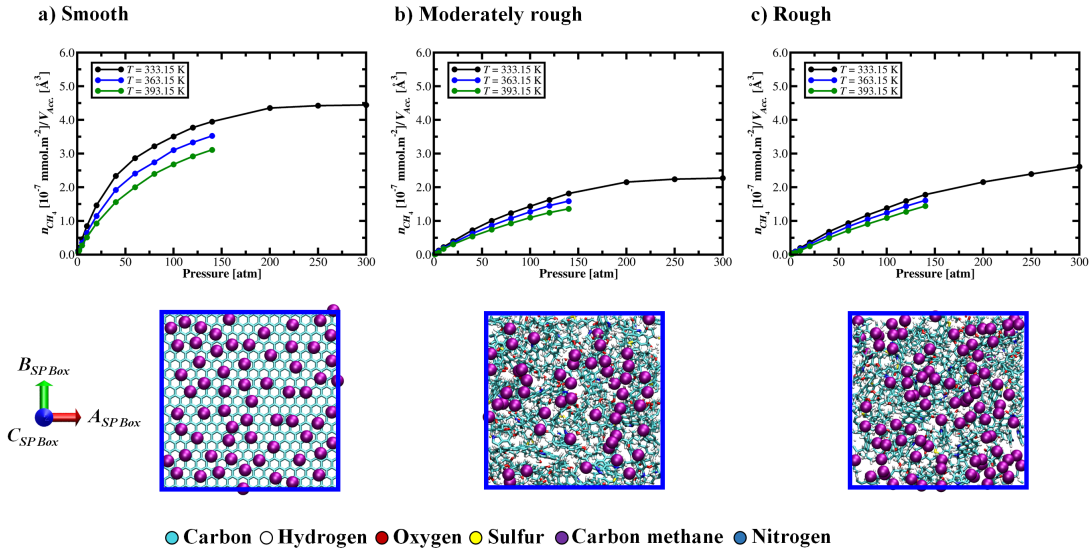

Figure S9: Methane absolute adsorption normalized by the accessible volume in the adsorption layer in the: a) rigid smooth slit nanopore, b) moderately rough rigid slit nanopore, and c) rough rigid slit nanopore at different temperatures. The snapshots correspond to the surfaces in the A_{SPBox}- and B_{SPBox}-direction at $P = 300$ atm from rigid systems.

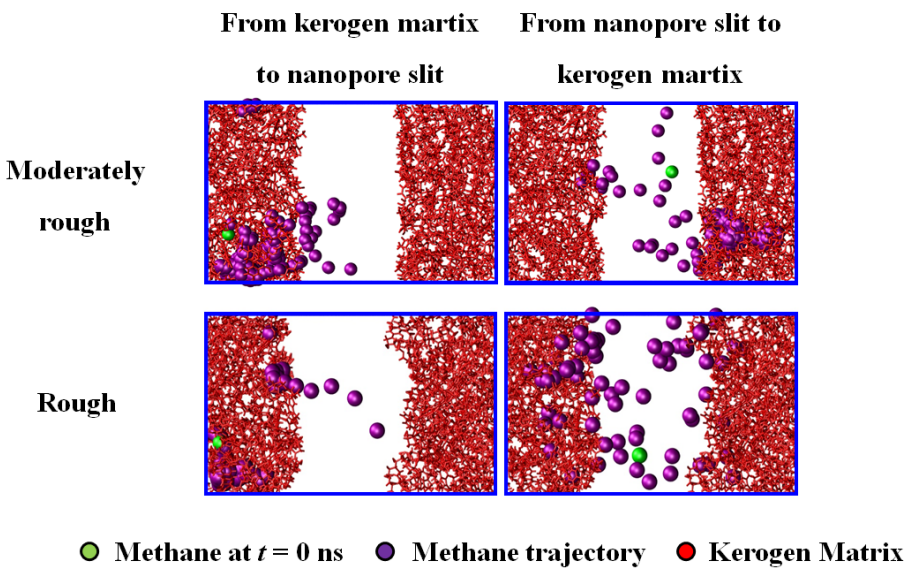

Figure S10: Tracked methane molecule in the moderately rough and rough flexible slit nanopores at $T = 333.15$ K and $P = 140$ atm.

References

(1) Ungerer, P.; Collell, J.; Yiannourakou, M. Molecular modeling of the volumetric and thermodynamic properties of kerogen: Influence of organic type and maturity. *Energ. Fuel.* **2014**, *29*, 91–105.

(2) Isothermal properties for methane. `https://www.nist.gov/`, (accessed December 19, 2017).

(3) Ozdemir, E.; Morsi, B. I.; Schroeder, K. Importance of volume effects to adsorption isotherms of carbon dioxide on coals. *Langmuir* **2003**, *19*, 9764–9773.

(4) Yang, F.; Ning, Z.; Zhang, R.; Zhao, H.; Krooss, B. M. Investigations on the methane sorption capacity of marine shales from sichuan basin, china. *Int. J. Coal Geol.* **2015**, *146*, 104–117.

(5) Tian, H.; Li, T.; Zhang, T.; Xiao, X. Characterization of methane adsorption on over-mature lower silurian–upper ordovician shales in sichuan basin, southwest china: Experimental results and geological implications. *Int. J. Coal Geol.* **2016**, *156*, 36–49.

(6) Zhao, T.; Li, X.; Ning, Z.; Zhao, H.; Li, M. Molecular simulation of methane adsorption on type II kerogen with the impact of water content. *J. Pet. Sci. Eng.* **2017**, 302–310.

(7) Zhao, T.; Li, X.; Zhao, H.; Li, M. Molecular simulation of adsorption and thermodynamic properties on type II kerogen: Influence of maturity and moisture content. *Fuel* **2017**, *190*, 198–207.

(8) Huang, L.; Ning, Z.; Wang, Q.; Qi, R.; Zeng, Y.; Qin, H.; Ye, H.; Zhang, W. Molecular simulation of adsorption behaviors of methane, carbon dioxide and their mixtures on kerogen: Effect of kerogen maturity and moisture content. *Fuel* **2018**, *211*, 159–172.